scientific reports

Check for updates

OPEN

Fast–slow dynamics in a cyanobacteria–phosphorus model

Hamid Abdolabadi[1]✉, Emad Mahjoobi[2] & Laleh Divband Hafshejani[1]

Understanding how cyanobacterial blooms emerge from biological processes requires models that account for both rapid physiological adjustments and slower nutrient dynamics. In this study, we analyze a cyanobacterial-phosphorus model using dynamic simulation, quasi-steady-state approximation (QSSA), single-parameter sensitivity analysis, and global uncertainty propagation. Comparisons between the full model and QSSA show that while QSSA can reproduce the rapid equilibrium of the internal phosphorus quota, it systematically overestimates dissolved phosphorus during periods of high external loading because it ignores short-term biomass-nutrient feedbacks. Sensitivity analyses reveal threshold-like transitions in biomass behavior for initial biomass and growth rate. The model abruptly shifts from low steady state biomass to one in which biomass grows rapidly. In a broader parameter set, the model indicates two qualitatively distinct long-term states. A low-biomass, light-limited state and a high-biomass, bloom-prone state reflect the existence of a bifurcated structure in the ecological dynamics. Uncertainty analysis confirms the coexistence of two distinct dynamical states including rapid collapse to a low-biomass state and sustained convergence toward a high-biomass attractor under combinations of growth capacity, light availability, and nutrient loading. Partial rank correlation analysis identifies growth rate and light attenuation as dominant controls on bloom magnitude, while nutrient storage parameters exert secondary influence. This study indicates that cyanobacterial model can experience ecological bifurcations, where small changes in environmental or physiological conditions shift the ecosystem between alternative stable states. Therefore, we show a vital characteristic of such models by combining fast–slow analysis, sensitivity analysis, and global uncertainty propagation which is crucial for studying eutrophication and designing effective nutrient management strategies.

Keywords Algal bloom model, Quasi-steady-state approximation, Sensitivity analysis, Uncertainty propagation

Blooming of cyanobacteria is becoming more of a concern for worldwide aquatic ecosystems. Nutrient enrichment, along with climate change, is increasing cyanobacteria and their impact[1]. Toxic blooms decrease water quality, deplete oxygen, disrupt aquatic food webs, and increase the cost of water treatment. They also threaten human health and the health of entire ecosystems[2,3]. Negative economic impacts due to cyanobacterial harmful algal blooms (CHABs) include loss of recreational and tourism opportunities, and the health risks CHABs pose when water used for irrigation of crops is contaminated[4,5]. CHAB formation and persistence are usually dependent on the availability of nutrients, especially phosphorus, which is often the key limiting nutrient in freshwater systems[6,7]. However, the relationship between nutrient availability and CHABs dynamics is more complex than simply considering the effect of external nutrient concentrations. Cyanobacteria have internal nutrient storage systems that enable them to grow even when external nutrient levels appear low[8]. This feature provides the potential for rapid development of algal blooms and eutrophication in aquatic environments. This process is influenced by intracellular nutrient quotas, referring to the ratio of internal nutrient content to cellular biomass, which can change significantly based on environmental conditions[9,10].

Stoichiometry can help explain links between nutrient–growth relationships in ecological systems[11,12]. This is particularly relevant for phytoplankton dynamics, integrating cellular processes such as nutrient acquisition and storage with growth and competitive dominance[13,14]. It highlights that organisms do not passively absorb nutrients but flexibly adjust their internal composition, modifying growth and ecological success. Recent research in stoichiometric models advances simplistic constant nutrient ratios toward flexible internal quotas and variable uptake rates[13,15]. These developments improve understanding of transient dynamics in bloom formation, where rapid changes in internal nutrient concentration allow sudden growth under favorable conditions[16,17]. Multi-

[1]Department of Environmental Engineering, Faculty of Water and Environmental Engineering, Shahid Chamran University of Ahvaz, Ahvaz, Iran. [2]Department of Water and Environmental Engineering, Faculty of Civil Engineering, Shahrood University of Technology, Shahrood, Iran. ✉email: h.abdolabadi@scu.ac.ir

scale analysis has been useful in characterizing parameter regimes supporting rapid blooms, and in describing lags between uptake, growth, and nutrient depletion[7].

Integrating internal phosphorus quota dynamics and external nutrient availability is essential for understanding CHAB formation. The Droop model links internal nutrient quotas to growth rate, and remains foundational in phytoplankton modeling, emphasizing internal nutrient storage as the ultimate constraint while uptake depends on both external concentration and cellular quota[18–20]. Nevertheless, much remains unknown about nutrient–algal interactions in CHABs. The spatial-temporal dynamics of these interactions are often poorly represented. Internal quota regulation operates on hours-to-days scales, whereas ecosystem nutrient cycles evolve seasonally or annually. This mismatch in timescales is central to the challenge.

Recent experimental work highlights further complexities that must be integrated into coupled models. Multiple timescales generate behavioral complexity, including oscillations and abrupt shifts between equilibria[21–23]. Understanding these dynamics is fundamental for predicting bloom timing and designing interventions, as management actions can produce very different outcomes depending on system state[24,25]. Mathematical tools such as sensitivity analysis and multi-scale techniques provide promising routes to identify parameter thresholds underlying rapid transitions[26]. From a management perspective, coupled models which incorporates internal phosphorus dynamics outperform traditional models by considering lag times caused by nutrient reductions, addressing internal loading, and assessing intervention impacts[27,28].

Our literature review reveals that most cyanobacteria–phosphorus models have focused on equilibrium behavior, single deterministic trajectories, or steady-state nutrient–biomass relationships in lake ecology. As a result, comparatively little attention has been given to how fast physiological processes (such as internal nutrient storage and growth) interact with slow ecosystem-scale nutrient dynamics to shape transient behavior, regime selection, and long-term system outcomes, specifically under realistic parameter uncertainty. In addition, quasi–steady-state reductions do not explicitly account for evaluating how the removal of fast transients alters nutrient–biomass feedbacks. Therefore, it remains unclear whether commonly used mechanistic models can reveal distinct regime changes, or how sensitive such regimes are to growth capacity, light limitation, and nutrient loading.

In this study, we address this gap by combining full dynamic simulations, fast–slow analysis, sensitivity experiments, and global uncertainty propagation in a physiologically structured cyanobacteria–phosphorus model. Rather than focusing solely on equilibrium solutions, we examine transient dynamics across a broad parameter space. This approach reveals the presence of alternative biomass regimes from low-biomass to bloom-prone or high-biomass states suggesting bifurcation-like behavior driven by interactions between growth, light availability, and nutrient supply. By identifying the processes that govern regime selection and quantifying how uncertainty propagates through the system, this work provides new mechanistic insight into threshold behavior in cyanobacterial bloom dynamics and highlights the importance of timescale interactions in eutrophication modeling.

Methodology

Ecological modeling framework

To investigate the ecological dynamics of cyanobacteria and phosphorus under seasonal forcing, the mechanistic, stoichiometric model based on cell-quota formulation was used[9,18]. The model represents the coupled dynamics of algal biomass $B(\mathrm{gC\,m^{-3}})$, internal cellular phosphorus quota $Q(\mathrm{gP\,g^{-1}C})$, and dissolved inorganic phosphorus $P(\mathrm{gP\,m^{-3}})$ within a well-mixed epilimnion layer of depth z_m (m).

The dimensional model equations are:

$$\frac{dB}{dt} = B\left[\mu\left(Q,B\right) - \nu_r - k_f\right] \tag{1}$$

$$\frac{dQ}{dt} = \rho\left(P,Q\right) - \mu\left(Q,B\right)Q \tag{2}$$

$$\frac{dP}{dt} = I\left(t\right) - k_f P - B\rho\left(P,Q\right) \tag{3}$$

where t is time (days), $\mu\left(Q,B\right)$ is the specific growth rate $\left(\mathrm{d^{-1}}\right)$, $\rho\left(P,Q\right)$ is the phosphorus uptake rate $\left(\mathrm{gP\,g^{-1}C\,d^{-1}}\right)$, ν_r is the respiration/mortality rate $\left(\mathrm{d^{-1}}\right)$, $k_f = D/z_m$ is the flushing rate $\left(\mathrm{d^{-1}}\right)$, $I\left(t\right)$ is the external phosphorus load $\left(\mathrm{gP\,m^{-3}d^{-1}}\right)$, modeled as a sinusoidal function to represent seasonal variability.

The growth rate depends on the internal quota Q:

$$\mu\left(Q,B\right) = \begin{cases} r\left(1 - \frac{Q_m}{Q}\right)h\left(B\right), & Q > Q_m \\ 0, & Q \le Q_m \end{cases} \tag{4}$$

where r is the maximum specific growth rate ($\mathrm{d^{-1}}$), and Q_m is the minimum subsistence quota ($\mathrm{gP\,g^{-1}C}$). The light limitation function $h\left(B\right)$ represents vertical light attenuation due to background turbidity and self-shading[24]:

$$h\left(B\right) = \frac{1}{z_m K_T\left(B\right)} \ln\left(\frac{H + I_{\mathrm{in}}}{H + I_{\mathrm{in}} e^{-K_T(B) z_m}}\right) \tag{5}$$

$$K_T(B) = K_{\mathrm{bg}} + kB \tag{6}$$

where $K_{\mathrm{bg}}\left(\mathrm{m}^{-1}\right)$ is the background light extinction, $k\left(\mathrm{m}^2\mathrm{g}^{-1}\mathrm{C}\right)$ is the specific light attenuation by biomass, I_{in} is incident irradiance (μ mol $\mathrm{m}^{-2}\mathrm{s}^{-1}$), and H is the half-saturation constant for light limitation (μ mol m^{-2} s^{-1}).

The phosphorus uptake rate follows a Michaelis–Menten form with an upper quota limitation:

$$\rho(P,Q) = \rho_m \frac{P}{M+P}\left(1 - \frac{Q}{Q_M}\right) \tag{7}$$

where ρ_m is the maximum uptake rate $\left(\mathrm{gP}^{-1}\,\mathrm{C\,d}^{-1}\right)$, M is the half-saturation constant for phosphorus uptake (gP m^{-3}), and Q_M is the maximum internal quota (gP g^{-1}C).

The external phosphorus load $I(t)$ is defined as a seasonal sinusoid:

$$I(t) = I_{\mathrm{mean}} + A_I \sin\left(\frac{2\pi\, t}{T_p}\right) \tag{8}$$

where I_{mean} $\left(\mathrm{gP\ m}^{-3}\mathrm{d}^{-1}\right)$ is the annual mean load, A_I is its amplitude, and T_p is the annual period (days).

Quasi–steady state analysis (QSSA)

The cyanobacterial–phosphorus system exhibits processes on disparate timescales. Fast variables including B and Q controlled by rapid physiological responses (growth and uptake). However, a slow variable like P is influenced by external forcing and cumulative biomass feedbacks[28].

The QSSA assumes that B and Q reach a local steady state relative to the slower dynamics of P. Setting $dB/dt = dQ/dt = 0$ in Eqs. (1) and (2) yields:

$$0 = B(\mu(Q,B) - \nu_r - k_f) \tag{9}$$

$$0 = \rho(P,Q) - \mu(Q,B)Q \tag{10}$$

The first equation gives a condition for equilibrium growth:

$$\mu(Q,B) = \nu_r + k_f \tag{11}$$

which can be substituted into the second to obtain $Q^*(P)$. Combining Eqs. (4)-(8) gives an implicit relation between Q and P:

$$\rho_m \frac{P}{M+P}\left(1 - \frac{Q}{Q_M}\right) = Q(\nu_r + k_f) \tag{12}$$

Equation (12) can be solved numerically for $Q^*(P)$. The steady biomass B^* is obtained from Eq. (11) and the light limitation function $h(B)$:

$$h\left(B^*\right) = \frac{\nu_r + k_f}{r\left(1 - \frac{Q_m}{Q^*(P)}\right)} \tag{13}$$

Substituting $B^*(P)$ and $Q^*(P)$ into the slow equation for P yields a one-dimensional slow manifold:

$$\frac{dP}{dt} = I(t) - k_f P - B^*(P)\,\rho\left(P, Q^*(P)\right) \tag{14}$$

This reduced form allows analytical inspection of phosphorus persistence and sensitivity to seasonal load variation without simulating full three-variable dynamics.

Sensitivity analysis

To evaluate the response of the system to initial conditions and key physiological parameters, a local–global sensitivity analysis was performed. We varied initial biomass B_0 $\left(0.01 - 100\mathrm{gC\ m}^{-3}\right)$ and initial phosphorus P_0 $\left(0.1 - 1\mathrm{gP\ m}^{-3}\right)$ in logarithmic steps, solving Eqs. (1)-(3) for 730 days. Sensitivity was quantified by the elasticity of peak biomass to initial value:

$$S_{B_0} = \frac{\Delta \ln(\mathrm{peak}B)}{\Delta \ln(B_0)} \tag{15}$$

Four key parameters were analyzed: the growth rate (r_s), uptake rate (ρ_m), and nutrient states (B and P). Each parameter (p_i) was altered by $\pm 20\%$ around its nominal value while others were fixed, and the normalized sensitivity coefficient was computed:

$$S_{p_i}^X = \frac{p_i}{\overline{X}} \frac{\partial \overline{X}}{\partial p_i} \approx \frac{p_i}{\overline{X}} \frac{X(p_i + \Delta p_i) - X(p_i - \Delta p_i)}{2\Delta p_i} \tag{16}$$

where X denotes an output metric (peak B, mean B, or final P) and $\overline{X}$ is its baseline value. The analysis was implemented numerically using centered finite differences.

Uncertainty analysis

To propagate parametric uncertainty through the ecological model, a Latin Hypercube Sampling (LHS) approach was used[29]. The uncertain parameters were sampled from prescribed probability distributions. For each ensemble member i, the model (Eqs. 1–3) was integrated over $t \in [0,730]$ days using ODE15s. Output statistics such as peak biomass, final biomass, mean biomass over the last year, time to bloom, and time to periodic steady-state were extracted.

Let $\mathbf{p}^{(i)} = [r, \rho_m, Q_m, Q_M, k, K_{\mathrm{bg}}, M, A_I]^{(i)}$ denote the parameter vector of run i. The ensemble means and quantile envelopes were computed as:

$$\overline{X}(t) = \frac{1}{N} \sum_{i=1}^{N} X^{(i)}(t), \; X_{p,q}(t) = \mathrm{Quantile}_{p,q}\left(\left\{X^{(i)}(t)\right\}_{i=1}^{N}\right) \tag{17}$$

for percentiles $p = 5, q = 95$.

Partial rank correlation coefficients (PRCC) between ranked inputs and outputs were used to assess global sensitivities[26]:

$$\mathrm{PRCC}_{j,k} = \mathrm{corr}\left(r_{x_j} - \hat{r}_{x_j}, r_{y_k} - \hat{r}_{y_k}\right) \tag{18}$$

where r_{x_j} and r_{y_k} are rank-transformed variables and hats denote residuals from multiple linear regressions excluding the j^{th} variable. Significant PRCC values ($|\mathrm{PRCC}| > 0.3, \mathrm{p} < 0.05$) identify dominant parameters affecting model responses.

Model parameters and simulation

We used MATLAB 2012 to solve deferential equations with ODE15s. Table 1 shows all the parameters and sources used to simulate the full dynamic model.

Results and discussion

At first step, the dynamic behaviors of biomass B(t), internal phosphorus quota Q(t), and dissolved phosphorus P(t) are simulated in two forms of the full three-variable ODE system and the quasi–steady-state approximation (QSSA) for one 365 days under a sinusoidal external phosphorus input (Fig. 1).

The full ODE simulation shows a rapid decline in cyanobacterial biomass during the first 40 days, decreasing from an initially high value (1 g C m^{-3}) to a very low equilibrium state (0.2 g C m^{-3}). The QSSA biomass trajectory is essentially flat at this low equilibrium value throughout the year. This occurs because the QSSA assumes that

Symbol	Parameter	Unit	Nominal value	Range	Source
r	Max. growth rate	d^{-1}	1	0.5–2.0.5.0	Reynolds[9]; Jöhnk et al[24].
Q_m	Min. quota	gP g^{-1}C	0.004	0.002–0.008	Droop[18]; Huisman et al[1].
Q_M	Max. quota	gP g^{-1}C	0.04	0.02–0.06	Droop[18]
ν_r	Respiration/mortality	d^{-1}	0.35	0.2–0.5	Reynolds[9]
K_{bg}	Background light extinction	m^{-1}	0.3	0.2–0.6	Jöhnk et al[24].; Staehr et al[30].
k	Self-shading coefficient	m^2 g^{-1}C	0.4×10^{-3}	0.0002 – 0.0008	Jöhnk et al[24].
I_{in}	Incident irradiance	µmol m^{-2} s^{-1}	300	200–500	Sterner & Elser[31]
H	Light half-saturation	µmol m^{-2} s^{-1}	120	100–200	Huisman et al[1].
ρ_m	Max. uptake rate	gP g^{-1}C d^{-1}	1	0.5–2.0.5.0	Reynolds[9]
M	Half-sat. const. for uptake	gP m^{-3}	1.5×10^{-3}	0.0005 – 0.003	Salmaso[32]
D	Water inflow rate	m d^{-1}	0.02	0.01–0.05	Field estimates
z_m	Mixed-layer depth	m	7	5–10	Local monitoring
k_f	Flushing rate D/z_m	d^{-1}	0.0029	0.001–0.007	Computed
A_I	Forcing amplitude	gP m^{-3} d^{-1}	0.77	0.3–1.0.3.0	Seasonal load data
I_{mean}	Mean forcing	gP m^{-3} d^{-1}	0.77	0.3–1.0.3.0	Seasonal load data
T_p	Forcing period	days	365	—	Annual cycle

Table 1. Model parameters and sources.

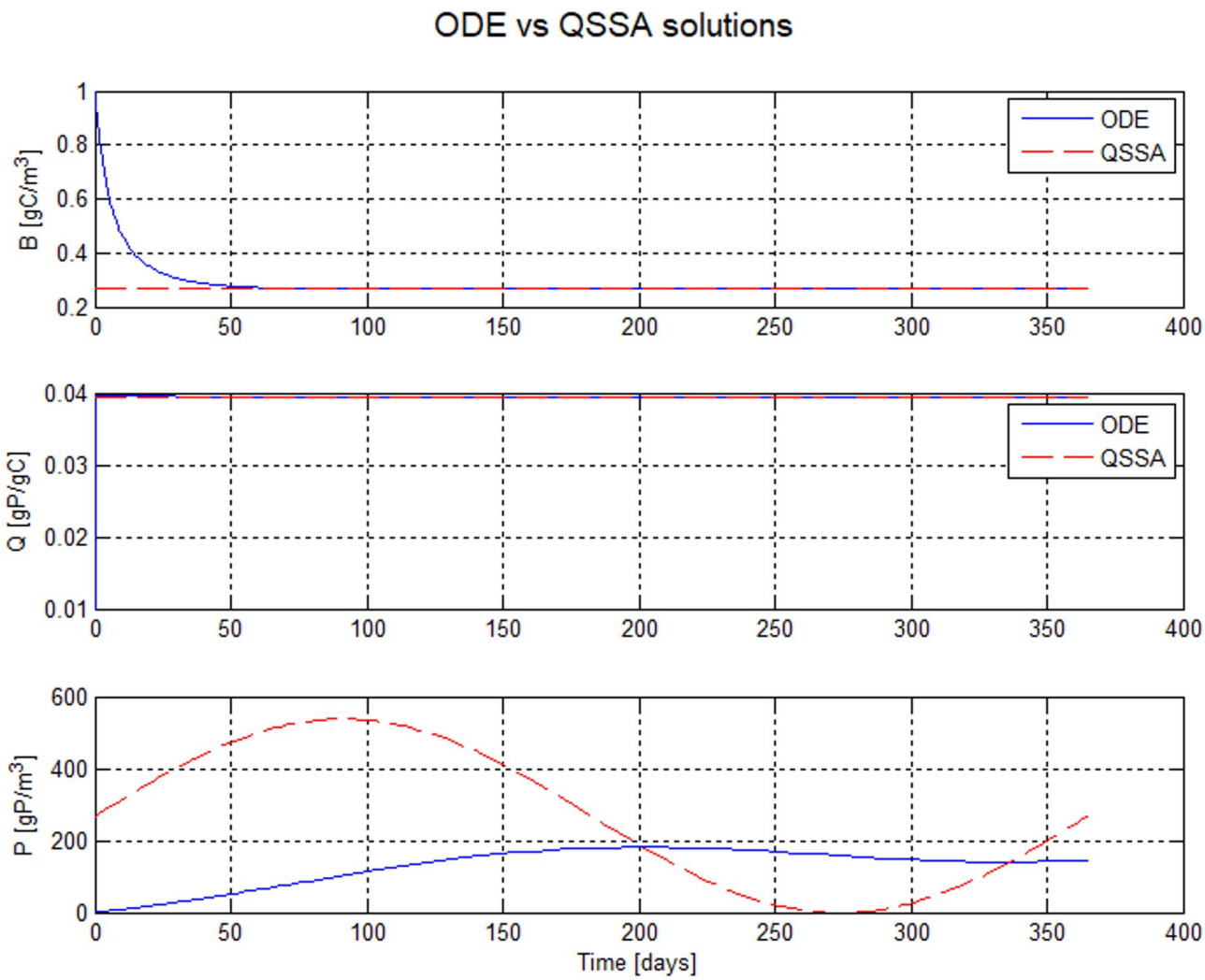

Fig. 1. Simulation results for the full three-variable ODE system and the QSSA for 365 days.

biomass instantaneously equilibrates to conditions determined by the slowly varying phosphorus concentration. The full model reveals a short fast transient driven by rapid physiological turnover in B and Q, whereas the QSSA explicitly removes these transients. The internal quota Q(t) in the full ODE simulation, quickly increases toward the upper physiological bound Q_M and remains at this maximum throughout almost the entire simulation. This saturation of the quota arises due to the external phosphorus and a fast uptake relative to growth (high ρ_m compared to μ). The QSSA reproduces this behavior almost exactly. Because the quota is a fast variable, it rapidly adjusts to the slow state of phosphorus availability.

The greatest discrepancy between the two modeling approaches is in the dissolved phosphorus P(t). In the dynamic model, phosphorus shows a gradual increase through the year, rising from near zero to roughly 180 mg m^{-3} by day 200. This slow accumulation reflects the balance between external loading and weak uptake by the biomass. However, the QSSA solution produces a much stronger seasonal oscillation, with peak phosphorus concentrations exceeding 500 mg m^{-3}. The reason is that in the reduced QSSA system, biomass is held at its equilibrium, which changes only slowly. During periods of high external loading, the reduced biomass has insufficient uptake, and phosphorus rises more dramatically. After approximately day 200, both curves begin to converge as the phosphorus load decreases and the influence of uptake becomes more linear. This overestimation of phosphorus indicates a well-known effect of QSSA reductions. By removing transient biomass responses, the system underestimates the short-term feedback of algae on phosphorus, leading to exaggerated P excursions.

Sensitivity analysis

We performed a group of simulations of the cyanobacteria–phosphorus model based on varied initial biomass on a logarithmic grid from 0.01 to 1 gC m^{-3}. All other parameters and initial conditions are fixed. For each run we recorded the full time series of B(t), P(t), and Q(t) as well as the steady-state time. These steady times are marked as colored symbols on the time-series (Fig. 2). All trajectories for B collapse toward a common low steady biomass (0.266 g C m^{-3}) after an initial transient. For small B_0, the system shows a slow decay and long transient (many tens of days) before settling. For B_0 less than 0.26 gC m^{-3} the peak biomass is essentially insensitive to B_0

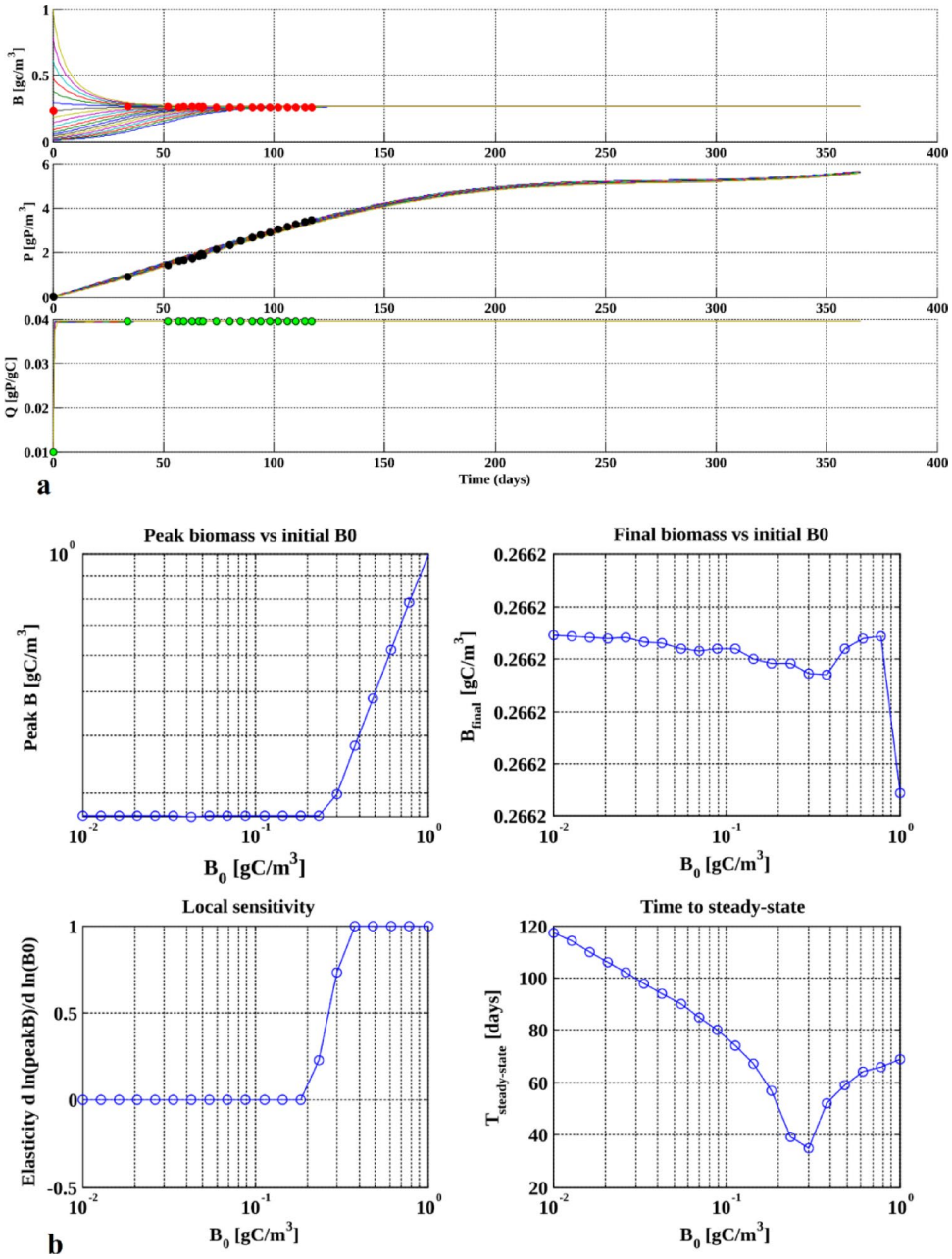

Fig. 2. Summary diagnostics computed for each run include peak biomass, final biomass, the local elasticity of peak biomass with respect to B_0, and steady-state time.

(the curve is flat and near zero), meaning the system's early dynamics do not amplify small initial biomass into large blooms. When initial biomass is small, uptake capacity $B\rho(P, Q)$ is small, therefore dissolved phosphorus accumulates driven by external loading before biomass can respond.

Quota rapidly saturates (fast variable), but growth $\mu(Q, B)$ remains small because B is small. Therefore, system's transient is governed by the slow P accumulation and biomass cannot amplify. Also, the local elasticity of peak biomass with respect to B_0 is zero in this regime. Practically, doubling B_0 results essentially no change in peak biomass. For larger B_0, some trajectories show a short transient before converging and biomass monotonically declines toward the same attractor.

The initial B_0 is the maximum for each run and consequently the measured peak increases with B_0. This is because a large initial biomass instantaneously provides uptake capacity and hence can temporarily depress P. In addition, other processes (respiration, flushing, light limitation) relax biomass downward to the attractor. There is no sustained positive feedback to maintain the large initial biomass: it is a transient seed. Elasticity rises toward 1 in this case. In other words, peaks scale roughly proportionally with B_0. The final biomass at the end varies only in the third or fourth decimal place (around 0.2662 gC m^{-3}) over the entire range of B_0. This means that despite large differences in early transient peaks, all trajectories converge to the same long-term attractor.

Figure 3 indicates that the biomass remains low and approaches the steady-state for low r slowly. Quotas rapidly saturate to Q_M, and phosphorus steadily accumulates because uptake is weak relative to input and flushing. For intermediate r, the trajectories show longer, sometimes oscillatory transients. Biomass can temporarily change before settling. The biomass steady marker moves right for some higher growth rates. As r increases, biomass often starts high and decays to the same attractor. The uptake is rapid and phosphorus levels remain lower (or rise less) than for small r. The growth rate r adjusts how quickly cells convert internal quota to biomass ($\mu = r(1 - Q_m/Q)h(B)$). When r is small, uptake is not translated rapidly into biomass and P accumulates leads to B stays low. When r is large, uptake can be consumed quickly, which transiently increases uptake capacity (but other losses still drive the long-term attractor).

Peak biomass is nearly constant at very low r, then there is an abrupt change around a critical r (about 1 d^{-1}). Therefore, it can be seen that there are two regimes. A low-r regime where the system cannot intensify biomass (peaks insensitive to r), and a regime around the critical r where dynamics change qualitatively.

The sharp change indicates a nonlinear response where small increases in r near that critical value produce large changes in observed peak biomass. Elasticity with respect to P_0 is near zero for low r. It will be negative and large in magnitude across the transition. This indicates that once the system is in the sensitive band, increases in r reduce the measured peak P. Elasticity with respect to B is near zero for low r and rises steeply in the threshold. Small changes in r lead to changes in peak biomass (elasticity > 1). The cyanobacterial respiration ν_r is varied across the range 0.05–0.6 d^{-1}. For each value, the full three-state model is performed. Figure 4 present the time series B(t), P(t), and Q(t) with summary of other metrics.

All state variables rapidly decline from the initial value and reach to a very similar low equilibrium (0.26 gC m^{-3}). As ν_r increases the early transient downfalls quickly but the time of steady-state condition (the red markers) moves to larger times. Dissolved P increases slowly during the simulation due to external loading and the relatively low uptake capacity. Q equilibrates extremely fast and is nearly saturated for all ν_r values. Increasing

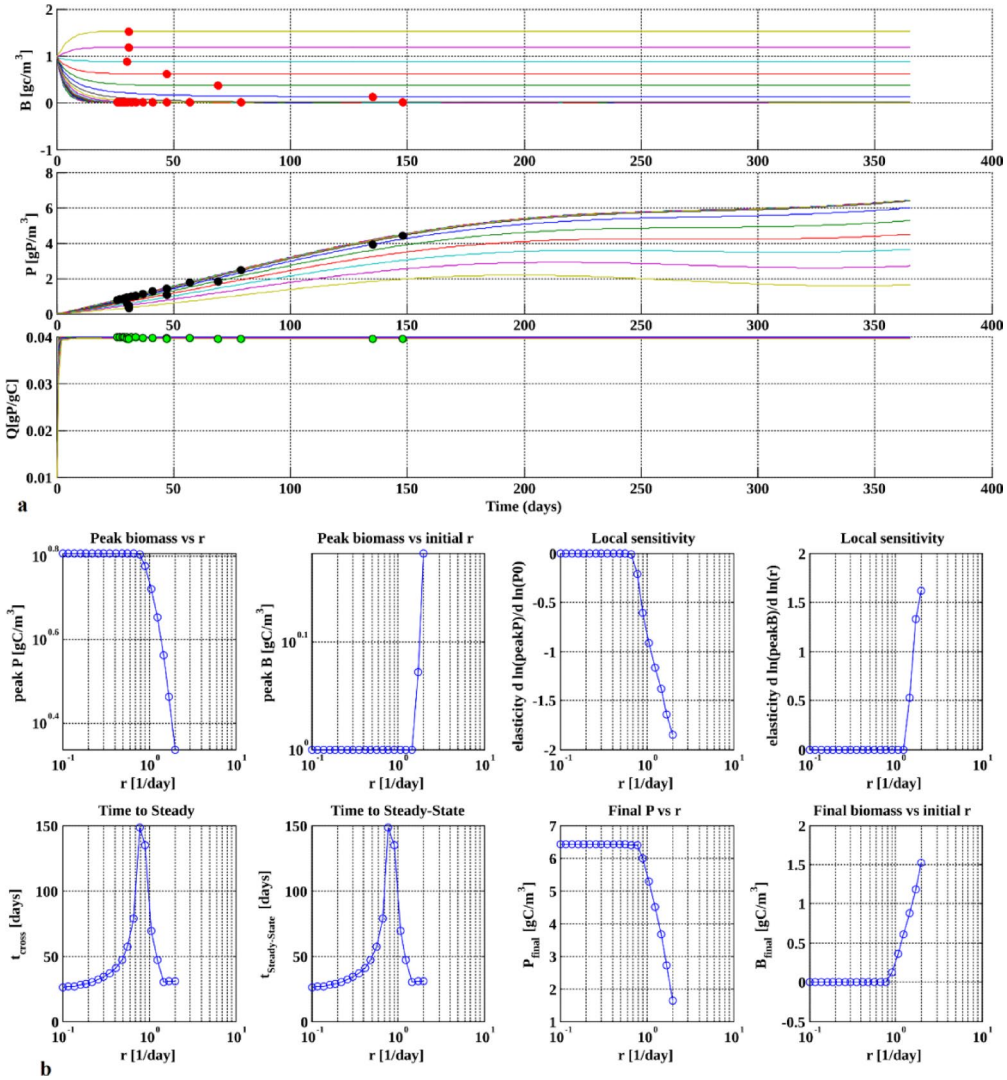

Fig. 3. Effect of varying growth rate r. For every simulation the red, black, and green markers show the time when biomass B first attains the steady.

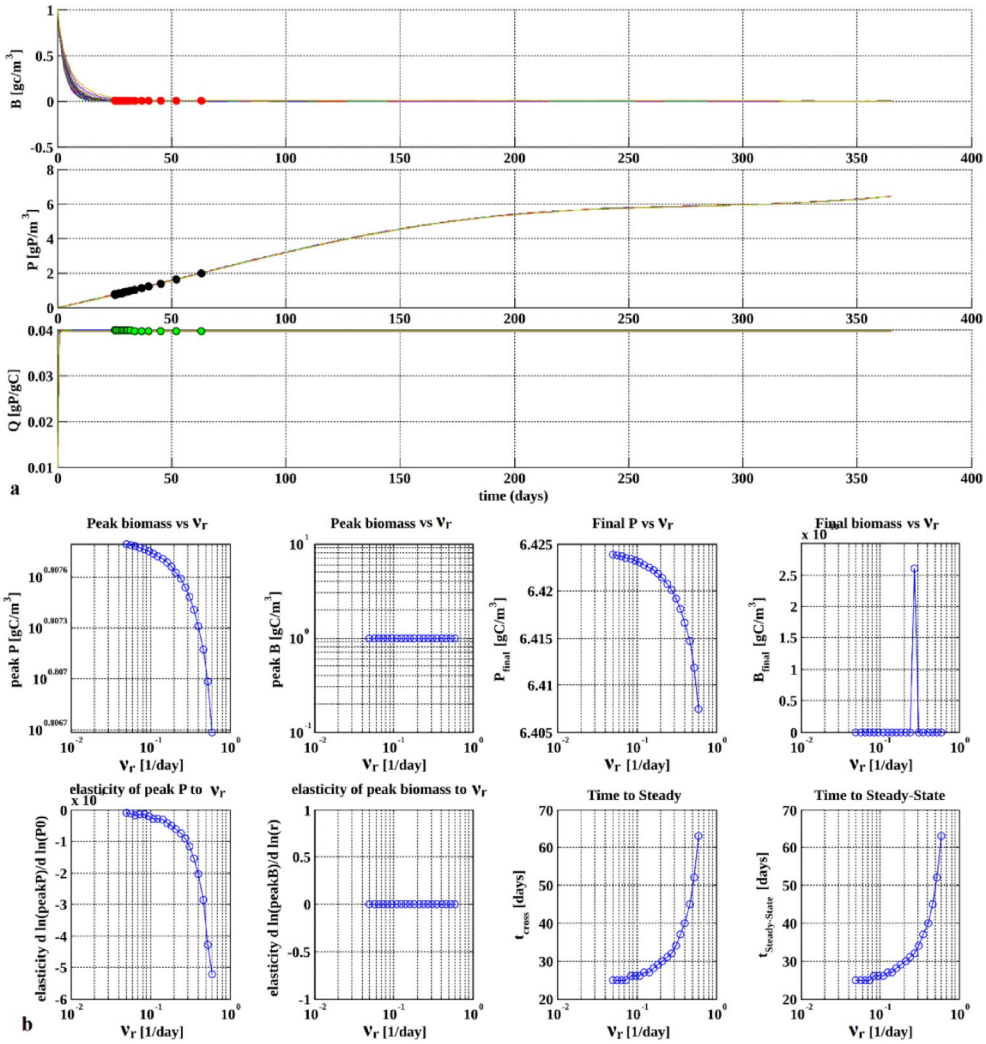

Fig. 4. B(t), P(t), and Q(t) for the sampled ν_r values. The eight subplots show how these metrics change across the ν_r.

respiration shifts the timescale on which biomass relaxes to the attractor but does not cause qualitatively different time series shapes. Increasing ν_r surges the loss term in the biomass equation, reducing net growth potential ($\mu - \nu_r - k_f$). Lower net growth reduces long-term biomass and thus the cumulative phosphorus uptake capacity. The observed small decrease in P_{max} and P_{final} with increasing ν_r indicates the net system response is that a higher loss rate actually slightly reduces P accumulation. The elasticity of P is negative across the range and its absolute magnitude increases as ν_r grows. A 1% increase in ν_r at high loss rates is associated with several percent decrease in P_{max}. The elasticity of B is approximately zero across the domain. Peak biomass does not respond (in proportional terms) to changes in ν_r as the initial value is the peak.

Uncertainty analysis

We applied uncertainty analysis in eight model parameters including maximum growth rate r, maximum P-uptake ρ_m, minimum quota Q_m, maximum quota Q_M, algal self-shading coefficient k, background light attenuation K_{bg}, P half-saturation M, and seasonal P loading amplitude AI using a Latin-hypercube. For each ensemble member the three-state model was simulated in 2 years with ODE15s. Summaries were computed as the sample median and the 5–95% quantile envelope. Global sensitivities of scalar outputs to inputs were evaluated with Partial Rank Correlation Coefficients (PRCCs). Figure 5 describes the principal results.

The uncertainty analysis reveals two fundamentally different attractor pathways for biomass. For most parameter samples, biomass has a rapid collapse during the first 20–40 days. It reaches a low steady-state around $0.2 - 0.3$ gC m^{-3} with the 5–95% envelope. In this condition, the regime corresponds to light limitation (high k or K_{bg}), insufficient physiological capacity (low r or low ρ_m), or strong losses. Another trend can be seen as high-biomass convergence. Here, the subset of simulations indicates the opposite behavior. Biomass does not decline. Instead, B increases over time from its initial value. Trajectories converge toward a high steady-state value, exceeding B = 1 gC m^{-3}. This corresponds to parameter combinations where growth capacity is strong

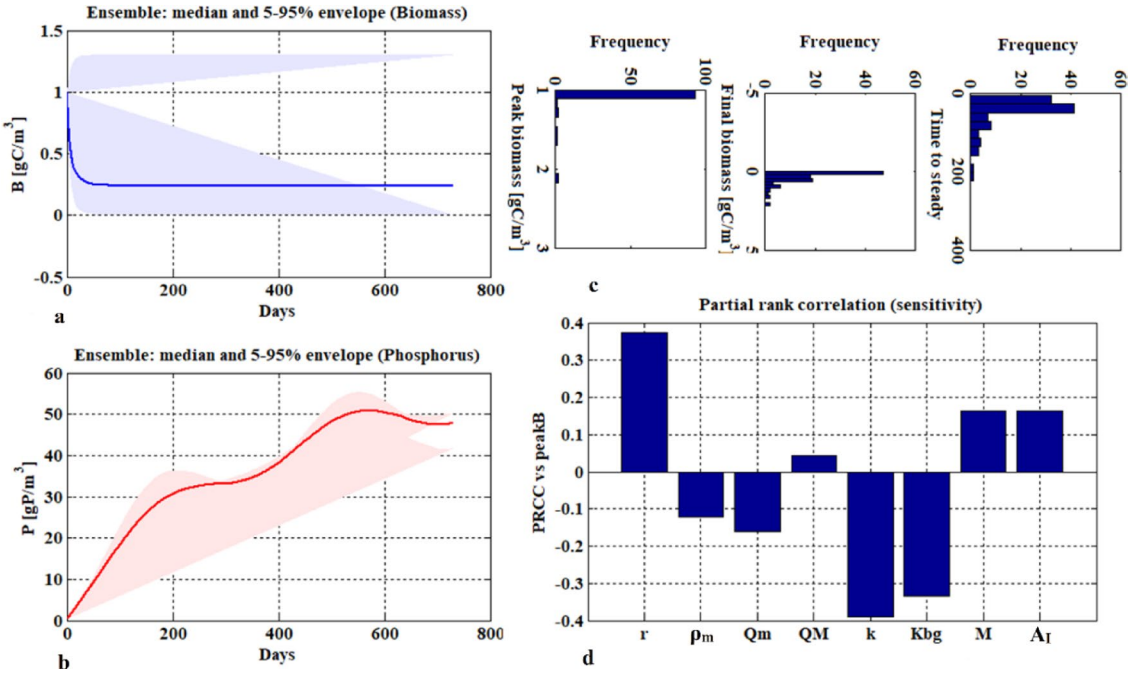

Fig. 5. Uncertainty analysis of the cyanobacteria–phosphorus model. Simulations (100 runs) show biomass B(t) and phosphorus P(t) with median and 5–95% envelopes (shading). Histograms summarize peak biomass, final biomass, and time to steady behavior. Partial rank correlation coefficients identify the dominant parameters.

(high r), light limitation is weak (low k and low K_{bg}), uptake is large (ρ_m), and seasonal P loading amplitude A_I is high. These conditions allow cyanobacteria to maintain positive net production.

The phosphorus increases continuously over the two-year simulation and the 5–95% envelope widens with time as external loading accumulates. This indicates that while biomass uncertainty decreases over time, uncertainty in dissolved P increases. The Peak biomass histogram indicates that in most simulations, the initial value is the peak. It means that changing the set of parameters leads to lower steady state biomass concentration. The final biomass distribution is narrow, indicating that almost all parameter combinations converge to similar final B values by the end of the simulation window. The time required for biomass to reach steady behavior exhibits a broader distribution. Many simulations settle within a range of 10–100 days, but a non-negligible fraction require much longer. This reflects parameter combinations that weaken the fast-stabilizing feedback (e.g., high loss rates or strong light attenuation) and therefore slow convergence.

The PRCC bar chart quantifies partial correlations between each input parameter and the output peak biomass. Statistically significant and practically important correlations can be inferred where absolute PRCC is large (conventionally |PRCC|>0.3) and p-values are small. PRCC for r is positive and strong (0.35). Higher growth rate increases the peak biomass. This is expected when physiological growth capacity is larger. ρ_m is slight negative which means that greater uptake capacity reduces the available external phosphorus, which tends to lower peak biomass. This implies strong uptake efficiency decreases bloom magnitude.

PRCC for Q_m is weak negative presenting a higher minimum quota reduces specific growth ($1 - Q_m/Q$ becomes smaller), thereby decreasing peak biomass. Similarly, Q_M is small negative. It shows that slightly larger storage capacity has a minor negative association with peak biomass. This effect is small and likely parameter-interaction dependent. Larger self-shading reduces light penetration and growth, substantially reducing peak biomass. Thus, k is strongly negative and is one of the most influential parameters. like k, higher background turbidity lowers light availability and strongly reduces peak biomass (K_{bg} is strongly negative). Its magnitude is comparable to k and thus both light-related parameters dominate negative sensitivity. Increasing M raises the external P level needed to saturate uptake. It reduces uptake efficiency at low P and allows larger peaks. Stronger seasonal loading increases available P and thereby peak biomass (moderate positive PRCC).

Biological perspective

The full cyanobacteria–phosphorus model reveals an early transient that is absent from the quasi–steady-state approximation. When initialized with relatively high biomass, cyanobacteria rapidly decline during the first 30–40 days, after which biomass stabilizes at a low state. Biologically, this initial collapse reflects the mismatch between uptake capacity and environmental constraints. Although internal phosphorus quota increases quickly due to rapid uptake, growth remains limited by light attenuation, respiration, and flushing losses. As a result, stored phosphorus cannot be efficiently converted into new biomass, leading to a net decline.

The QSSA removes this transient entirely by assuming that biomass instantaneously adjusts to the slowly varying nutrient environment. While this assumption indicates the fast equilibration of internal quota, it

suppresses the short-term feedback between biomass and phosphorus uptake. Consequently, QSSA simulations exaggerate dissolved phosphorus accumulation during periods of high external loading, because the temporary uptake capacity provided by transient biomass is effectively ignored. From a biological perspective, this implies that reduced models may overestimate nutrient concentrations during bloom onset or collapse phases, even if long-term averages are well captured.

Varying the initial biomass over two orders of magnitude reveals a striking contrast between short-term sensitivity and long-term resilience. This ecologically indicates that small cyanobacteria concentrations do not necessarily trigger blooms, even under favorable nutrient inputs. In contrast, when initial biomass is large, it immediately provides substantial uptake capacity and transiently suppresses dissolved phosphorus. However, this advantage is short-lived. Light limitation, respiration, and flushing rapidly reduce biomass, and all trajectories ultimately converge to the same low seasonal attractor. In this regime, the initial biomass simply defines the peak value, and elasticity approaches unity.

Changing the maximum growth rate reveals a nonlinear transition in system behavior. Biologically, this behavior reflects an ecological threshold. A minimum physiological growth capacity is required for cyanobacteria to exploit available nutrients. Below this threshold, blooms cannot form regardless of nutrient supply. Near the threshold, the system becomes highly sensitive to environmental variability, consistent with observed interannual bloom variability in lakes with similar nutrient loads.

In contrast to growth rate, increasing cyanobacterial respiration does not alter the qualitative structure of biomass trajectories. Instead, it modifies the rate at which the system approaches equilibrium. From a biological perspective, respiration acts as a damping mechanism that weakens population resilience without changing the ecological regime. This suggests that management actions increasing loss processes (e.g., grazing, flushing) may delay bloom recovery but are unlikely to shift the system into an alternative stable state on their own.

The PRCC analysis identifies light attenuation and growth rate as the dominant controls on peak biomass. Parameters governing light availability employ strong negative influence, confirming that light limitation remains a primary constraint on cyanobacterial blooms even in nutrient-rich systems. Growth rate exerts a strong positive influence, reinforcing the importance of physiological traits and temperature-dependent processes. Nutrient uptake parameters affect phosphorus accumulation rather than biomass amplification, highlighting a separation between drivers of bloom intensity and drivers of nutrient cycling.

Conclusion

This study applies to understand how a cyanobacteria–phosphorus model behaves under realistic environmental forcing, and how its predictions respond to uncertainty in ecological parameters and initial conditions. By combining dynamical analysis, sensitivity analysis, and global uncertainty propagation, we aimed to reveal not only what the model predicts, but how it behaves and which processes govern its. The comparison between the full ODE system and the QSSA reduction provided the first clear insight. Although the QSSA captured fast physiological equilibrium of the internal phosphorus quota, it systematically misrepresented the transient interactions between biomass and nutrients. The full model presented a rapid 40-day decline in biomass followed by slow re-equilibration driven by the interplay of uptake, growth, and light limitation. QSSA, by construction, removed this transient entirely, holding biomass too close to its long-term equilibrium. As a result, the reduced system exaggerated dissolved phosphorus excursions because it did not account for short-lived but ecologically important feedbacks between biomass and nutrient uptake. This mismatch highlights that while QSSA is valuable for long-term or equilibrium analyses, transient dynamics in eutrophication processes cannot be safely ignored when management-relevant time horizons (weeks to months) are considered.

The single-parameter sensitivity analyses acknowledges that small variations in initial conditions or growth parameters can lead to qualitatively different transient behaviors. Varying the initial biomass showed that the system is robust in the long run but early responses depend strongly on initial conditions. When initial biomass is small, the system behaves passively. In this regime, elasticity of peak biomass with respect to the initial biomass was essentially zero. For example, doubling the initial concentration barely altered the bloom. Peak biomass scaled roughly proportionally with B_0, and elasticity approached one. But none of these initial differences changed the long-term outcome. Varying the growth rate r revealed the presence of threshold-like behaviors. At low r, biomass remained at low values and the peaks were insensitive to changes in growth rate. However, around a critical value, the model showed a sharp transition where small increases in r caused large changes in the biomass peak. This nonlinear response is characteristic of trophic thresholds, where systems switch abruptly between low and high biomass states. In contrast, the respiration parameter ν_r changes the time scale rather than the trend. As respiration increases, biomass initially decreases more rapidly and then tends toward a steady state.

The uncertainty analysis combined all these findings and revealed a key conclusion. The model allows for two distinct regimes depending on the combination of physiological and environmental parameters. Most parameter sets produced a clear outcome (low biomass after the initial decline) that was consistent with the results of the sensitivity analyses. But a smaller subset of simulations showed that biomass steadily increased toward a steady-state of high biomass of more than 1 gC/m^3. This bifurcation naturally arises from interactions between light limitation, growth capacity, nutrient uptake, and phosphorus loading. In other words, the model predicts that lakes can be in a clear-water state or in a bloom-prone state, depending on the confluence of environmental forces and physiological characteristics. Soluble phosphorus behaved differently. The uncertainty increased over time as phosphorus accumulated in the system at rates dependent on the parameters. PRCC-based analysis helped explain why two regimes of low-biomass and high-biomass are established. Growth rate and light limitation parameters recognized as the key controls on peak biomass. Severe light attenuation significantly reduced growth. Uptake parameters shaped soluble phosphorus trends but played a secondary role in determining peak biomass. Together, these results suggest that light availability and physiological growth potential are key levers

governing biomass growth, while nutrient uptake kinetics and the external load primarily influence long-term phosphorus accumulation.

The findings of this study suggest that management interventions should be based on a careful assessment of the effectiveness of nutrient control scenarios, taking into account the dynamics and the possibility of biomass concentrations reaching different steady state concentrations as small changes in some parameters can lead to drastic changes in the state of the system. Finally, this simulation and uncertainty analysis demonstrate both the flexibility and fragility of cyanobacterial systems. The possibility of two steady states of low and high cyanobacterial concentrations in the system should be seriously considered in devising an effective plan.

Several limitations in the present framework should be acknowledged. The model is spatially homogeneous and therefore does not take into account vertical stratification, or sediment–water interactions that are known to influence cyanobacterial dynamics in real lakes. Important biological processes such as grazing, internal nutrient loading from sediments, and explicit temperature dependence are also omitted. In addition, the emergence of alternative biomass regimes is identified numerically through transient dynamics and sensitivity patterns rather than by formal bifurcation analysis. These limitations point toward future work, including the extension of the model to stratified or spatially explicit systems, incorporation of temperature- and food-web processes. Coupling such mechanistic models with long-term monitoring data may further enable early detection of regime shifts and improve the predictability of algal bloom.

Data availability

All data generated or analyzed during this study are included in this published article.

Received: 29 November 2025; Accepted: 31 December 2025
Published online: 07 January 2026

References

1. Huisman, J. et al. Cyanobacterial blooms. *Annu Rev. Environ. Resour.* **43**, (2018).
2. Paerl, H. W. et al. Mitigating cyanobacterial harmful algal blooms in aquatic ecosystems impacted by climate change and anthropogenic nutrients. *Harmful Algae*. **54**, 213–222 (2016).
3. Annual Review of Environment and Resources. Harmful cyanobacterial blooms: biological traits, mechanisms, risks, and control strategies. *Annu Rev. Environ. Resour.* **48**, (2023).
4. Vu, H. P., Nguyen, L. N., Zdarta, J., Nga, T. T. V. & Nghiem, L. D. Blue–green algae in surface water: problems and opportunities. *Curr. Pollut Rep.* **6**, 105–122 (2020).
5. Yang, Y. et al. Eutrophication promotes resource use efficiency and toxin production of *Microcystis* in a future climate warming scenario. *Environ. Res.* **261**, 120219 (2024).
6. Kong, X., Zhan, Q., Boehrer, B. & Rinke, K. Synergistic effects of warming and internal nutrient loading interfere with the long-term stability of lake restoration and induce sudden re-eutrophication. *Environ. Sci. Technol.* **57**, 2732–2742 (2023).
7. Zhang, H. et al. Climate and nutrient-driven regime shifts of cyanobacterial communities in low-latitude plateau lakes. *Environ. Sci. Technol.* **55**, 3408–3418 (2021).
8. Burford, M. A. et al. Advancing the research agenda for improving Understanding of cyanobacteria in a future of global change. *Harmful Algae*. **91**, 101601 (2020).
9. Reynolds, C. S. *The Ecology of Phytoplankton* (Cambridge Univ. Press, 2006).
10. Klausmeier, C. A., Litchman, E., Daufresne, T. & Levin, S. A. Optimal nitrogen-to-phosphorus stoichiometry of phytoplankton. *Nature* **429**, 171–174 (2004).
11. Klausmeier, C. A., Litchman, E. & Levin, S. A. A model of flexible uptake of two essential resources. *J. Theor. Biol.* **246**, 278–289 (2007).
12. Abdolabadi, H. & Latif, S. D. Trophic predictability analysis: employing constancy and contingency—A case study of Ilam reservoir. *J. Clean. Prod.* **471**, 143325 (2024).
13. Serpico, J., Shen, Z. & Lewis, M. A. Decoding the spatial spread of cyanobacterial blooms in an epilimnion. *J. Math. Biol.* **90**, 1 (2025).
14. Litchman, E., Klausmeier, C. A., Schofield, O. M. & Falkowski, P. G. The role of functional traits and trade-offs in structuring phytoplankton communities: scaling from cellular to ecosystem level. *Ecol. Lett.* **10**, 1170–1181 (2007).
15. Abdolabadi, H., Sarang, A., Ardestani, M. & Mahjoobi, E. Eutrophication modeling using variable chlorophyll approach. *Int. J. Environ. Res.* **10**, 273–290 (2016).
16. Heggerud, C. M., Wang, H. & Lewis, M. A. Transient dynamics of a stoichiometric cyanobacteria model via multiple-scale analysis. *SIAM J. Appl. Math.* **80**, 1223–1246 (2020).
17. Wang, H., Heggerud, C. M. & Lewis, M. A. A mathematical model for the effects of nitrogen and phosphorus on algal blooms. *Int. J. Bifurcat. Chaos*. **29**, 1950129 (2019).
18. Droop, M. R. Vitamin B12 and marine ecology. IV. The kinetics of uptake, growth and Inhibition in *Monochrysis lutheri*. *J. Mar. Biol. Assoc. U K*. **48**, 689–733 (1968).
19. Caperon, J. Population growth response of *Isochrysis Galbana* to nitrate variation at limiting concentrations. *Ecology* **49**, 866–872 (1968).
20. Aksnes, D. L. & Egge, J. K. A theoretical model for nutrient uptake in phytoplankton. *Mar. Ecol. Prog Ser.* **70**, 65–72 (1991).
21. Carpenter, S. R., Kinne, O. & Wieser, W. *Regime Shifts in Lake Ecosystems: Pattern and Variation* (Int. Ecology Inst., 2003).
22. Holmes, M. H. *Introduction to Perturbation Methods*. (Springer, 2012).
23. Kim, J. et al. Key drivers of microcystin-producing cyanobacteria in South Korean eutrophic waters determined with data-driven models. *J. Environ. Manage.* **377**, 126616 (2025).
24. Jöhnk, K. D. et al. Summer heatwaves promote blooms of harmful cyanobacteria. *Glob Change Biol.* **14**, 495–512 (2008).
25. Paerl, H. W. et al. Mitigating a global expansion of toxic cyanobacterial blooms: confounding effects and challenges posed by climate change. *Mar. Freshw. Res.* **71**, 579–592 (2020).
26. Helton, J. C. & Davis, F. J. Latin hypercube sampling and the propagation of uncertainty in analyses of complex systems. *Reliab. Eng. Syst. Saf.* **81**, 23–69 (2003).
27. Gobler, C. J. et al. Sewage- and fertilizer-derived nutrients alter the intensity, diversity, and toxicity of harmful cyanobacterial blooms in eutrophic lakes. *Front. Microbiol.* **15**, 1464686 (2024).
28. Westermark, S. & Steuer, R. Toward multiscale models of cyanobacterial growth: a modular approach. *Front. Bioeng. Biotechnol.* **4**, 95 (2016).
29. Saltelli, A. et al. *Global Sensitivity Analysis: the Primer* (Wiley, 2008).

30. Staehr, P. A., Christensen, J. P. A., Batt, R. D. & Read, J. S. Ecosystem metabolism in a stratified lake. *Limnol. Oceanogr.* **57**, 1317–1330 (2012).
31. Sterner, R. W. & Elser, J. J. *Ecological Stoichiometry: the Biology of Elements from Molecules to the Biosphere* (Princeton Univ. Press, 2002).
32. Salmaso, N. Life strategies, dominance patterns and mechanisms promoting species coexistence along environmental gradients. In *Phytoplankton and Equilibrium Concept* (eds Naselli-Flores et al.) 13–36 (Springer, 2003).

Author contributions

Hamid Abdolabadi: Conceptualization, Methodology, Writing – Original. Emad Mahjoobi: Conceptualization, Investigation, Interpretation, Writing. Laleh Divband Hafshejani: Visualization, Writing – Review & Editing.

Declarations

Competing interests

The authors declare no competing interests.

Additional information

Correspondence and requests for materials should be addressed to H.A.

Reprints and permissions information is available at www.nature.com/reprints.

Publisher's note Springer Nature remains neutral with regard to jurisdictional claims in published maps and institutional affiliations.